Asymmetrically localized proteins stabilize basal bodies against ciliary beating forces

Brian A. Bayless,[1] Domenico F. Galati,[1] Anthony D. Junker,[1] Chelsea B. Backer,[2,3] Jacek Gaertig,[4] and Chad G. Pearson[1]

[1]Department of Cell and Developmental Biology, University of Colorado School of Medicine, Aurora, CO 80045
[2]Whitehead Institute for Biomedical Research, Cambridge, MA 02142
[3]Department of Biology, Massachusetts Institute of Technology, Cambridge, MA 02142
[4]Department of Cellular Biology, University of Georgia, Athens, GA 30602

Basal bodies are radially symmetric, microtubule-rich structures that nucleate and anchor motile cilia. Ciliary beating produces asymmetric mechanical forces that are resisted by basal bodies. To resist these forces, distinct regions within the basal body ultrastructure and the microtubules themselves must be stable. However, the molecular components that stabilize basal bodies remain poorly defined. Here, we determine that Fop1 functionally interacts with the established basal body stability components Bld10 and Poc1. We find that Fop1 and microtubule glutamylation incorporate into basal bodies at distinct stages of assembly, culminating in their asymmetric enrichment at specific triplet microtubule regions that are predicted to experience the greatest mechanical force from ciliary beating. Both Fop1 and microtubule glutamylation are required to stabilize basal bodies against ciliary beating forces. Our studies reveal that microtubule glutamylation and Bld10, Poc1, and Fop1 stabilize basal bodies against the forces produced by ciliary beating via distinct yet interdependent mechanisms.

Introduction

Motile cilia produce hydrodynamic forces for diverse functions including cellular motility and fluid flow (Marshall and Kintner, 2008). The ciliary axoneme generates hydrodynamic force by using axonemal dynein to slide nine doublet microtubules arranged around two single microtubules (Satir et al., 2014). This activity leads to a two-phase, asymmetric beat stroke. During the power stroke, the extended cilium moves perpendicular to the cell surface, whereas during the recovery stroke, the bent cilium moves parallel to the cell surface, thereby returning the cilium for another cycle. Although axonemal dynein is sufficient to undulate cilia, to generate effective fluid flow, ciliary forces must be coupled to the cell cortex.

Basal bodies (BBs) nucleate motile cilia and anchor them to the cell cortex. They comprise nine radially symmetric triplet microtubules organized around a cartwheel structure. Because the A and B tubules of BBs are continuous with the axoneme tubules, BBs directly experience cilia-generated forces (Dippell, 1968; Allen, 1969; Dirksen, 1971). In sperm flagella, where axonemal mechanics are best understood, the nine microtubule doublets effectively form two segments. As flagella beat, these segments slide ∼110 nm relative to each other in a piston-like fashion, which leads to symmetric compression and tension at the ciliary base (Lindemann et al., 1992; Vernon and Woolley, 2004; Riedel-Kruse et al., 2007). However, during ciliary beating, which is asymmetric, the greatest compressive and tensile forces are predicted to occur at the sides of the BB where the power stroke terminates and initiates, respectively. The BB structures and molecules that compensate for the forces produced by motile cilia are poorly defined.

Despite the persistent exposure to ciliary forces, BBs are stable (Brinkley and Cartwright, 1975; Bobinnec et al., 1998a; Abal et al., 2005; Kunimoto et al., 2012). This stability stems from two conserved aspects of BB organization. First, symmetrically localized proteins, such as Bld10 and Poc1, link the radially symmetric BB structural domains. Bld10 connects the spokes of the BB cartwheel to each of the nine triplet microtubules, whereas Poc1 is crucial for linking triplet microtubules to one another (Bayless et al., 2012; Meehl et al., 2016). In bld10Δ and poc1Δ *Tetrahymena thermophila* cells, ciliary beating causes BB disassembly and triplet microtubule loss from sites that experience the greatest compressive and tensile forces. The second aspect of BB stability stems from microtubule-associated proteins and tubulin posttranslational modifications (PTMs), such as glutamylation, that directly stabilize triplet microtubules (Magiera and Janke, 2014). Depletion of the microtubule-associated protein CAP350 renders centriole triplet microtubules sensitive to nocodazole (Le Clech,

Correspondence to Chad G. Pearson: chad.pearson@ucdenver.edu

Abbreviations used: BB, basal body; PEO, polyethylene oxide; PTM, posttranslational modification; SIM, structured illumination microscopy; WT, wild type.

The Rockefeller University Press $30.00
J. Cell Biol. Vol. 215 No. 4 457–466
https://doi.org/10.1083/jcb.201604135

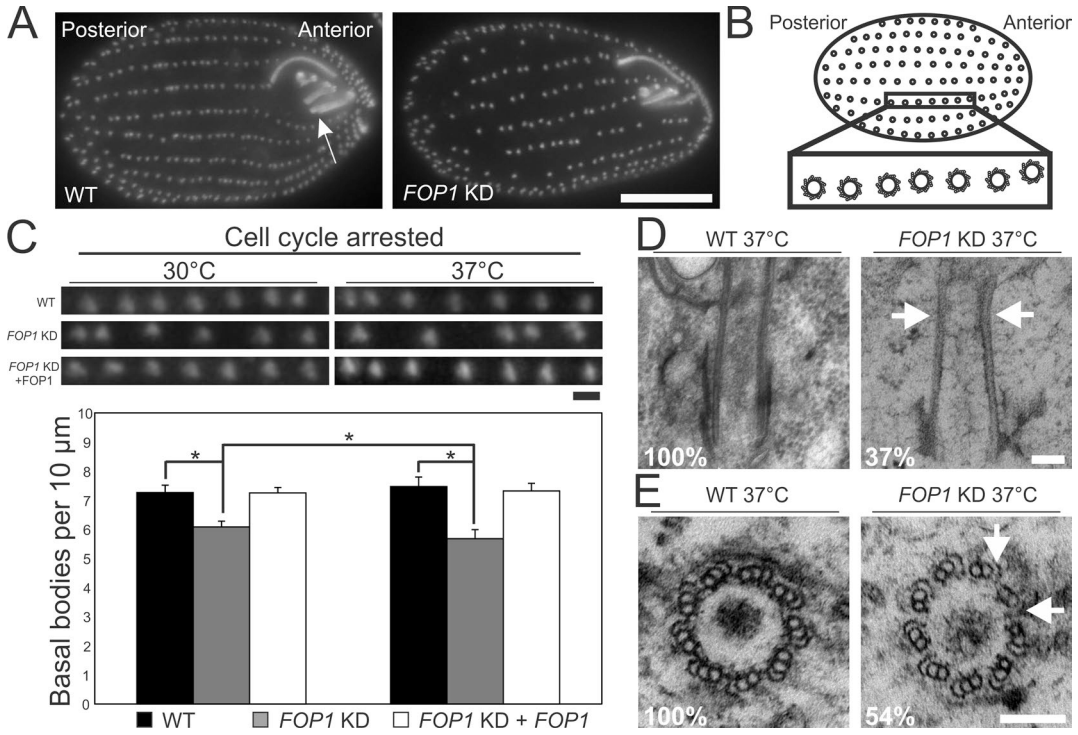

Figure 1. **Fop1 is a BB stability protein.** (A) Whole-cell BB immunofluorescence (α-centrin). *FOP1* knockdown (KD) cells have fewer BBs compared with wild type (WT). The cell's anterior is defined by the oral apparatus (arrow). Bar, 10 µm. (B) Schematic of a 10-µm segment of BBs along a ciliary row that represents the region used for BB frequency analysis. Bar, 1 µm. (C, top) *FOP1* KD cells have fewer BBs than WT cells. BB loss is rescued by the reintroduction of *FOP1*. Representative fluorescence images of BB rows in WT, *FOP1* KD, and *FOP1* KD with *FOP1* rescue at 30°C and 37°C in cell cycle arrested cells. (bottom) Quantification of BBs per 10 µm. Mean ± SEM; n = 300 rows; *, $P < 0.01$. (D and E) *FOP1* KD causes constricted BBs with defective C tubules (arrows). Electron micrographs of longitudinal (D) and cross-sectional (E) views of *FOP1* KD BBs at 37°C. n = 50 BBs for each orientation. Bars, 100 nm.

2008). Antibodies targeting microtubule glutamylation, which is prominent at axonemes and BBs, cause centriole fragmentation (Bobinnec et al., 1998a), whereas loss of the *Tetrahymena* tubulin glutamylases TTLL1 and TTLL9 leads to fewer ciliary rows and defects in BB maturation (Wloga et al., 2008). However, the interdependence of the various proteins and tubulin PTMs that stabilize BBs remains poorly defined. Moreover, it is unclear how these stability factors compensate for the asymmetric distribution of ciliary forces.

We identify the *Tetrahymena* FGFR1 oncogenic partner (Fop1) as a Bld10- and Poc1-associated protein required for BB stability. Both Fop1 and microtubule glutamylation are asymmetrically enriched at triplet microtubules predicted to experience the greatest compression forces from ciliary beating. Poc1 is necessary for normal Fop1 localization to BBs, whereas Poc1 and Fop1 levels affect BB microtubule glutamylation. These results suggest that cooperation between distinct pathways stabilizes BBs against ciliary forces.

Results and discussion

Fop1 is a BB stability protein

Candidate *Tetrahymena* BB stability proteins were identified by isolating Bld10- and Poc1-associated proteins (Tables S1, S2, and S3). 26 potential stability factors, including Fop1 (TTHERM_00537420), whose orthologues localize to centrosomes and function in microtubule anchoring, were identified (Mikolajka et al., 2006; Yan et al., 2006). To assess whether Fop1 stabilizes BBs, we depleted *FOP1* from *Tetrahymena* cells and quantified the linear density of BBs within the medial half of ciliary rows (Fig. 1, A and B; and Fig. S1, A–C). FOP1 knockdown reduces BB frequency by 16%, and, as observed for other BB stability proteins, increasing temperature exacerbates this defect (Fig. S1, C–E; 37°C; Pearson et al., 2009; Bayless et al., 2012). Because the number of ciliary rows remains constant, the reduced BB frequency represents actual BB loss (Fig. S1 G; Nanney and Chow, 1974).

BB loss could arise from reduced BB assembly through the cell cycle (Bayless et al., 2012). To test this, *FOP1* knockdown cells were starved, which arrests cells in G1 and halts new BB assembly (Figs. 1 C and S1 F). In selected G1 cells, there are 16% fewer BBs, which suggests that a fraction of BBs disassemble upon *FOP1* knockdown. To determine whether the remaining BBs exhibit structural defects, we examined the BB ultrastructure using EM. 37% of *FOP1* knockdown BBs have a reduced diameter or longitudinal tapering distal to the cartwheel (Figs. 1 D and S1 H). Moreover, 54% of BBs have C tubules that are missing or disconnected from their associated B tubules (Figs. 1 E and S1 I). Thus, Fop1 likely stabilizes BBs by promoting C-tubule formation and/or maintenance.

Fop1 stabilizes BBs from the forces of ciliary beating

Ciliary beating exerts forces on BBs, and these forces could precipitate BB structural defects and eventual disassembly. To test this, we manipulated ciliary beating after *FOP1* knockdown cells were cell cycle arrested. We used high temperature and increased media viscosity to elevate ciliary forces and $NiCl_2$ to inhibit ciliary beating, thereby decreasing forces at

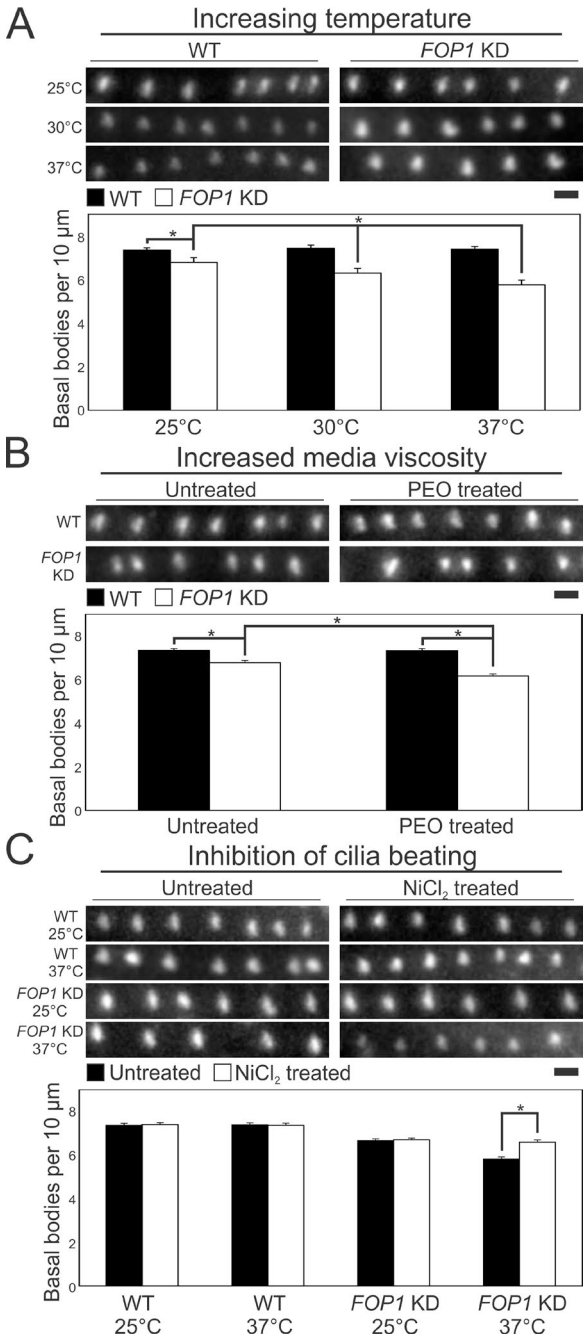

Figure 2. **Fop1 stabilizes BBs to resist ciliary beating.** (A) BB loss in *FOP1* KD cells is elevated at increasing temperatures. Representative BB rows (α-centrin) in WT and *FOP1* KD cells at 25°C, 30°C, and 37°C. (B) Increased media viscosity using PEO exacerbates the BB loss phenotype in *FOP1* KD cells. Representative BB rows in WT and *FOP1* KD cells in untreated or PEO media. (C) Inhibition of ciliary beating using $NiCl_2$ prevents high-temperature–induced BB loss in *FOP1* KD cells. Representative BB rows in WT and *FOP1* KD cells in untreated or $NiCl_2$-treated media. Mean ± SEM; n = 200 rows. *, $P < 0.01$. Bar, 1 µm.

BBs (Goto et al., 1982; Pearson et al., 2009). Both high temperature and viscous, polyethylene oxide (PEO)–containing media exacerbate BB loss in *FOP1* knockdown cells (Fig. 2, A and B). Conversely, $NiCl_2$ treatment rescues BB loss caused by shifting *FOP1* knockdown cells to 37°C (Fig. 2 C). These results suggest that Fop1 stabilizes BBs against the forces derived from ciliary beating.

Fop1 localizes asymmetrically to BBs

The *Tetrahymena* ciliary power stroke moves from the cell's anterior toward the posterior. Thus, the BB posterior face may experience asymmetric compressive force, whereas the anterior face experiences asymmetric tensile force. Because Fop1 stabilizes BBs, we asked whether Fop1 is asymmetrically positioned to reinforce the BB posterior and/or anterior faces. Endogenously tagged Fop1:mCherry localizes posteriorly relative to the centrally localized BB component Sas6a (Fig. 3 A). To quantify this localization, we determined the mean Fop1 signal relative to Sas6a, Cen1, and Poc1, which have known positions within the BB architecture (Fig. 3, B and C; and Fig. S2, A and B; Culver et al., 2009; Pearson et al., 2009). Indeed, fluorescence image averaging confirms that Fop1 is enriched at the posterior face of BBs. Furthermore, colocalization of N- and C-terminal–tagged Fop1 shows that the Fop1 protein is not extended or arranged in a polarized orientation (Fig. S2 C).

To examine the radial distribution of Fop1 at BBs, we used structured illumination microscopy (SIM; Fig. 3 D–F; and Fig. S2, D and F). Surprisingly, Fop1 variably localizes as horseshoe and ring shapes (Fig. 3 E). The angular displacement of the horseshoe varies and we predict that these localization patterns reflect dynamics of Fop1 protein within BBs. When the Fop1 SIM signal is averaged, the apex of the horseshoe preferentially localizes to the BB posterior face and, depending on the experiment, is slightly offset to triplet microtubules 1, 2, 8, and 9 (Fig. 3, B, D, and F; and Fig. S2, D and F). Linear and radial linescans reveal a second peak of lower intensity toward the anterior-facing triplet microtubules 3–5 that are often directly opposite to the posterior Fop1 signal. Subtle differences between imaging approaches may have resulted from minor deviations in sample alignment during averaging. Consistent with this result, immuno-EM shows a similar distribution (Figs. 3 G and S2 G). Collectively, Fop1 variably accumulates at BB regions predicted to experience the greatest compressive and tensile forces produced by ciliary beating.

A remaining question is how Fop1 is asymmetrically positioned to the posterior and anterior-facing triplet microtubules. One possibility is that the unequal forces generated by ciliary beating establish asymmetric cues for Fop1 localization. However, Fop1 is asymmetrically localized before ciliogenesis, although the level of Fop1 asymmetry increases with BB maturation and ciliary forces leading us to hypothesize that ciliary beating increases the asymmetric Fop1 localization (Fig. S2 E). Fop1 remains asymmetrically localized even when ciliary beating is inhibited (Fig. S2 F). This suggests that ciliary forces do not initiate or maintain asymmetric Fop1 localization. New BB assembly occurs from a predetermined triplet microtubule at the BB proximal end (O'Toole and Dutcher, 2014; Pearson, 2014), and BBs attach to the cellular cytoskeleton through structures that are asymmetric in their distribution (Bayless et al., 2016). Thus, the rotationally symmetric BB has inherent functional and structural asymmetries, and we predict that these preexisting asymmetries contribute to the asymmetric localization of Fop1.

Poc1 is necessary for normal incorporation of Fop1 into BBs

Poc1 uniformly localizes around the BB circumference; yet, in poc1Δ cells, posterior-facing triplet microtubules preferentially disassemble (Pearson et al., 2009; Meehl et al., 2016). Because Fop1 localizes to these same posterior-

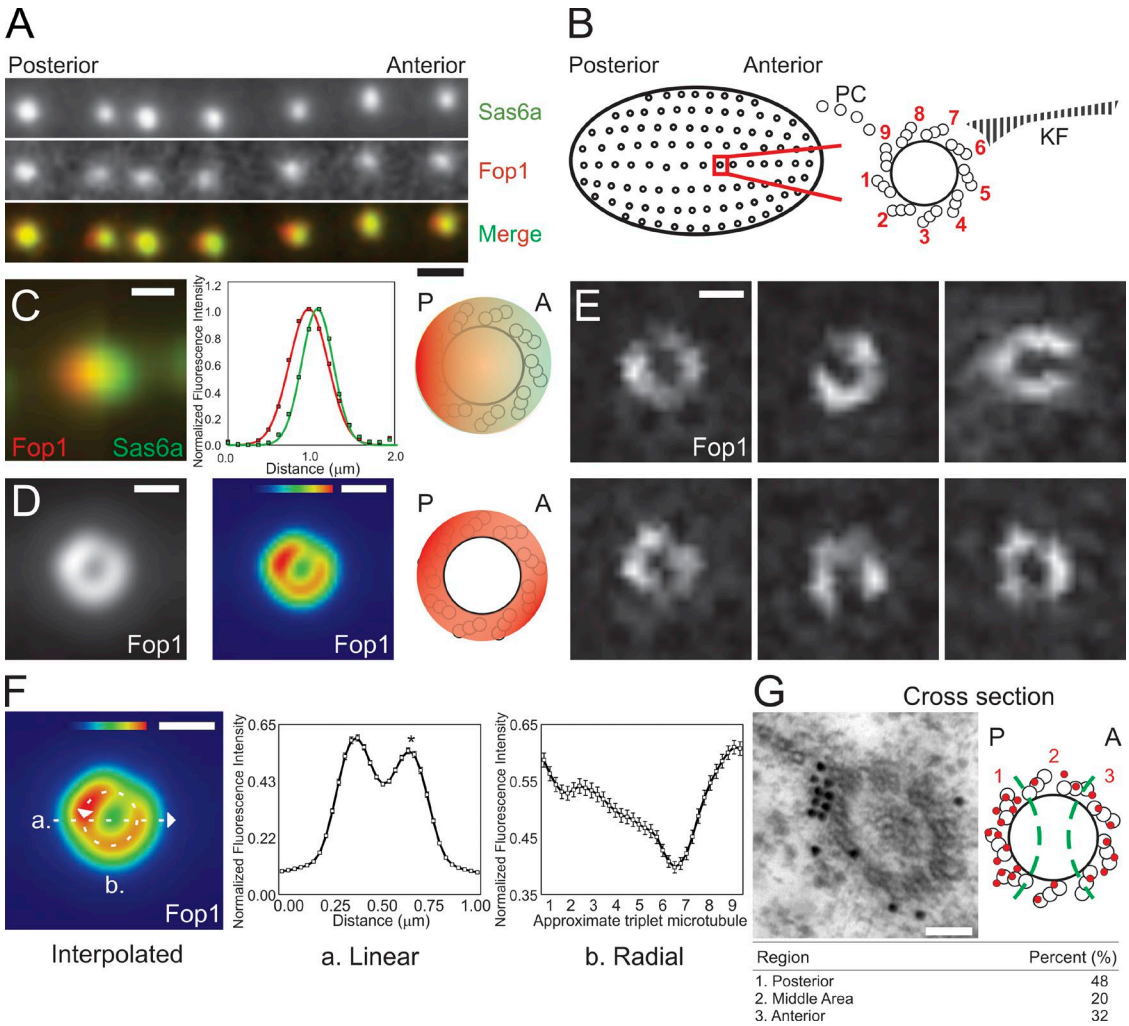

Figure 3. **Fop1 localizes asymmetrically at BBs.** (A) Fop1 is enriched at the posterior side of BBs. Inset of Sas6a-labeled (green; Sas6a:GFP) and Fop1-labeled (red; Fop1:mCherry) BBs. Bar, 1 µm. (B) Schematic showing a representative, polarized BB. KF, kinetodesmal fiber; PC, postciliary microtubules. (C) Fop1 is enriched at the posterior side of BBs. (left) Averaged two-color, colocalization of Fop1 (red) relative to centroid localizing, Sas6a (green). (middle) Linescan from a Gaussian fit curve to the mean localization. (right) Schematic representation of Fop1's BB localization. *n* = 45 BBs. Bar, 0.5 µm. (D, left) SIM image of Fop1's enrichment at the posterior (triplet microtubules 8 and 9) and anterior (triplet microtubules 4 and 5) triplet microtubules with an enrichment for posterior microtubules. Averaged SIM image of Fop1-labeled (red; Fop1:mCherry) BBs. *n* = 328 BBs. Bar, 0.25 µm. (middle) Heatmap illustrating intensity differences. (right) Schematic representation of Fop1 localization. (E) Representative SIM images showing dynamic Fop1 localization at individual BBs. Bar, 0.25 µm. (F, left) Interpolated intensity map of averaged Fop1 SIM images. Linear (middle) and radial (left) linescans. Arrow a in left panel corresponds to the linear linescan. Arrow b corresponds to the radial linescan. Asterisks denote levels distinct from posterior facing peak (*, $P < 0.01$). (G) Fop1:GFP immuno-EM localization in BB cross-sectional view. (right) Schematic of red dots denote Fop1's localization based on the relative distribution of 25 gold particles to represent the total quantified gold label. Numbers denote the region where Fop1 was measured. *n* = 125 gold particles in 21 BBs. Bar, 100 nm.

facing triplet microtubules, Poc1 and Fop1 may cooperatively stabilize this BB domain. To test such cooperativity, we measured Fop1:mCherry levels in poc1Δ cells. Fop1's levels do not change in poc1Δ cells, and, similarly, Poc1:mCherry levels do not change upon *FOP1* knockdown (Fig. 4 A). Thus, Poc1 and Fop1 are not required for each other's BB localization. To determine whether Poc1 and Fop1 can promote each other's BB incorporation, Poc1 or Fop1 was overexpressed and the BB levels of the reciprocal protein were measured. Poc1 overexpression increases Fop1 levels, whereas Fop1 overexpression does not change Poc1 BB levels (Figs. 4, B and C; and Fig. S2 I). This suggests that Poc1 promotes, but is not required for, Fop1 BB incorporation, and this functional interaction may impart stability to the posterior- and anterior-facing triplet microtubules.

There is a time delay between the start of BB assembly and the nucleation of a cilium, which provides a window to stabilize BBs before ciliary beating (Nanney, 1971; Bayless et al., 2012). Therefore, Poc1 may influence the timing of Fop1 incorporation to enhance BB stability before ciliary beating. To test this hypothesis, we measured the onset and subsequent maturation of endogenously tagged protein incorporation into BBs (Fig. 4, D–F). Daughter BBs form next to existing mother BBs and separate anteriorly as they mature. Thus, the distance between mother and daughter BBs is a proxy for BB maturation, and the protein fluorescence intensity ratio between the mother and daughter BBs reflects how much protein is incorporated during BB maturation. Fop1 incorporates early during BB assembly and levels increase rapidly during maturation, whereas Poc1 incorporates later and more slowly

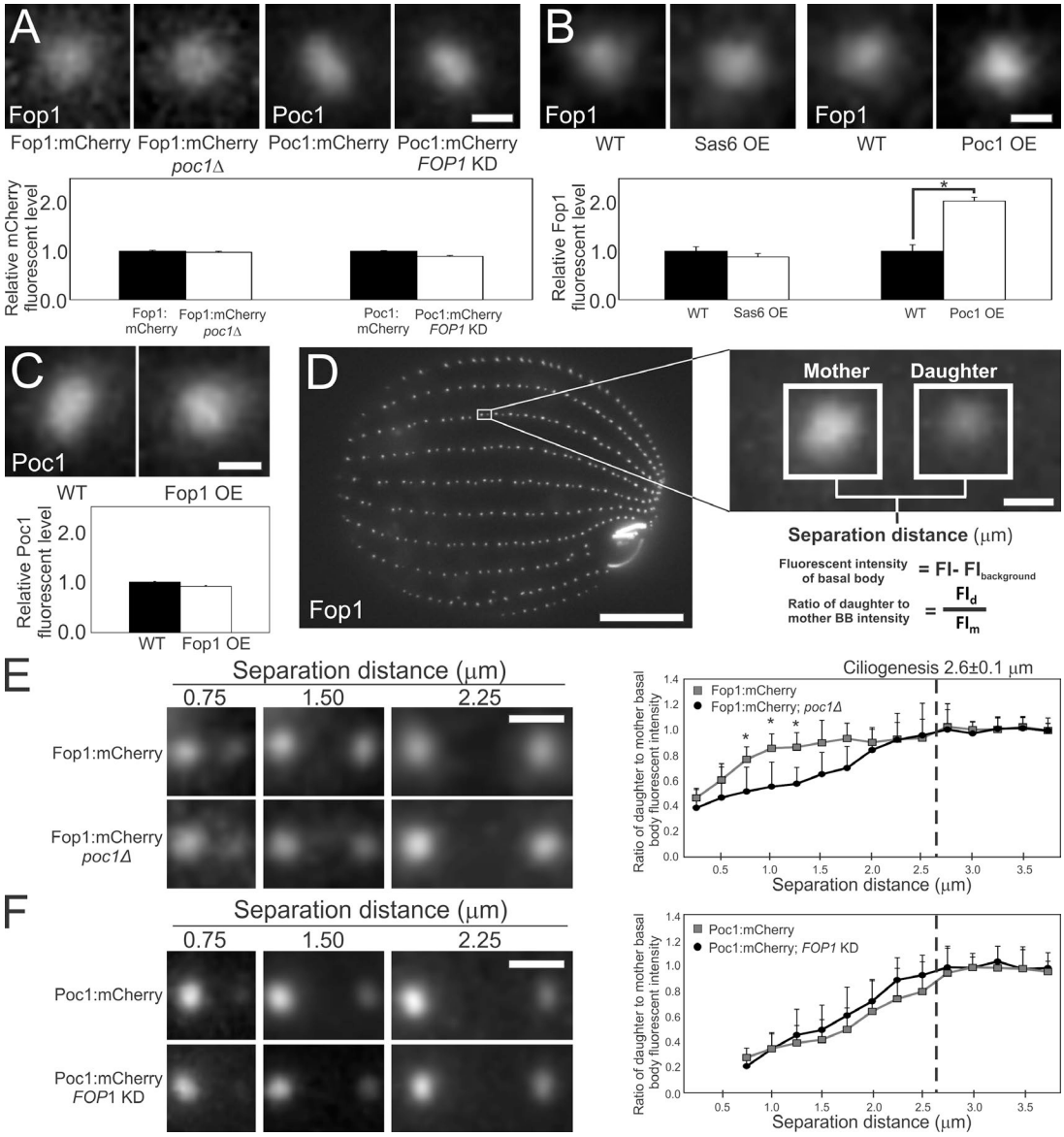

Figure 4. **Poc1 promotes normal Fop1 protein incorporation into BBs.** (A) Poc1 and Fop1 are not required for each other's localization to BBs. Poc1:mCherry or Fop1:mCherry BB levels do not change in response to knockdown or complete loss of the reciprocal protein, respectively. (B) Fop1 BB levels increase upon Poc1 overexpression (OE). Sas6a overexpression is a negative control. (C) Poc1 BB levels do not change upon Fop1 overexpression. (A–C) Bars, 0.5 µm. *n* = 150 BBs. (D) Representative Fop1:mCherry image denoting new BB assembly. Quantification of protein incorporation into new BBs is measured using the background-subtracted intensity levels of daughter BBs divided by mother BBs. This measurement is acquired relative to the separation distance of mother and daughter BBs. Bars: 10 µm; (inset) 0.5 µm. (E) The rate of Fop1 incorporation at new BBs decreases in poc1Δ cells. (left) Fop1 :mCherry levels relative to BB separation. (right) Quantification of Fop1:mCherry protein incorporation relative to mother-daughter BB separation distance. (F) Poc1:mCherry incorporation into BBs does not change in Fop1 KD cells. (left) Poc1:mCherry levels relative to BB separation. (right) Quantification of Poc1:mCherry protein incorporation relative to mother–daughter BB separation distance. (E and F) Dashed line represents mean distance upon which ciliogenesis occurs (2.6 ± 0.1 µm). Bars, 1 µm. Mean ± SEM; *, $P < 0.01$.

(Fig. 4, E and F). Both Poc1 and Fop1 reach complete protein levels before achieving the mean separation distance of BB ciliogenesis (2.6 ± 0.1 µm). This suggests that these stability factors incorporate before ciliary force generation (Fig. S2 H). Interestingly, Fop1 incorporates more slowly in poc1Δ cells, whereas Poc1 incorporation is not affected by *FOP1* knockdown (Fig. 4, E and F). These data are consistent with a model whereby a low level of symmetrically localized Poc1 facilitates the asymmetric recruitment of Fop1 to stabilize the posterior- and anterior-facing triplet microtubules of the BB in preparation for ciliary beating.

Microtubule glutamylation is asymmetrically enriched at and stabilizes BBs

BB and ciliary microtubules are posttranslationally modified by glutamylation. In flagellar axonemes, glutamylation asymmetrically localizes to the doublet microtubules that are in the plane of the ciliary beat stroke (Fouquet et al., 1996). It is not known whether such asymmetry exists at BBs, as observed for Fop1. To address this, we evaluated microtubule glutamylation via GT335 antibody staining. Glutamylated tubulin is found along the entire longitudinal length of the triplet microtubules. However, glutamylation is radially concentrated at the posterior-facing triplet

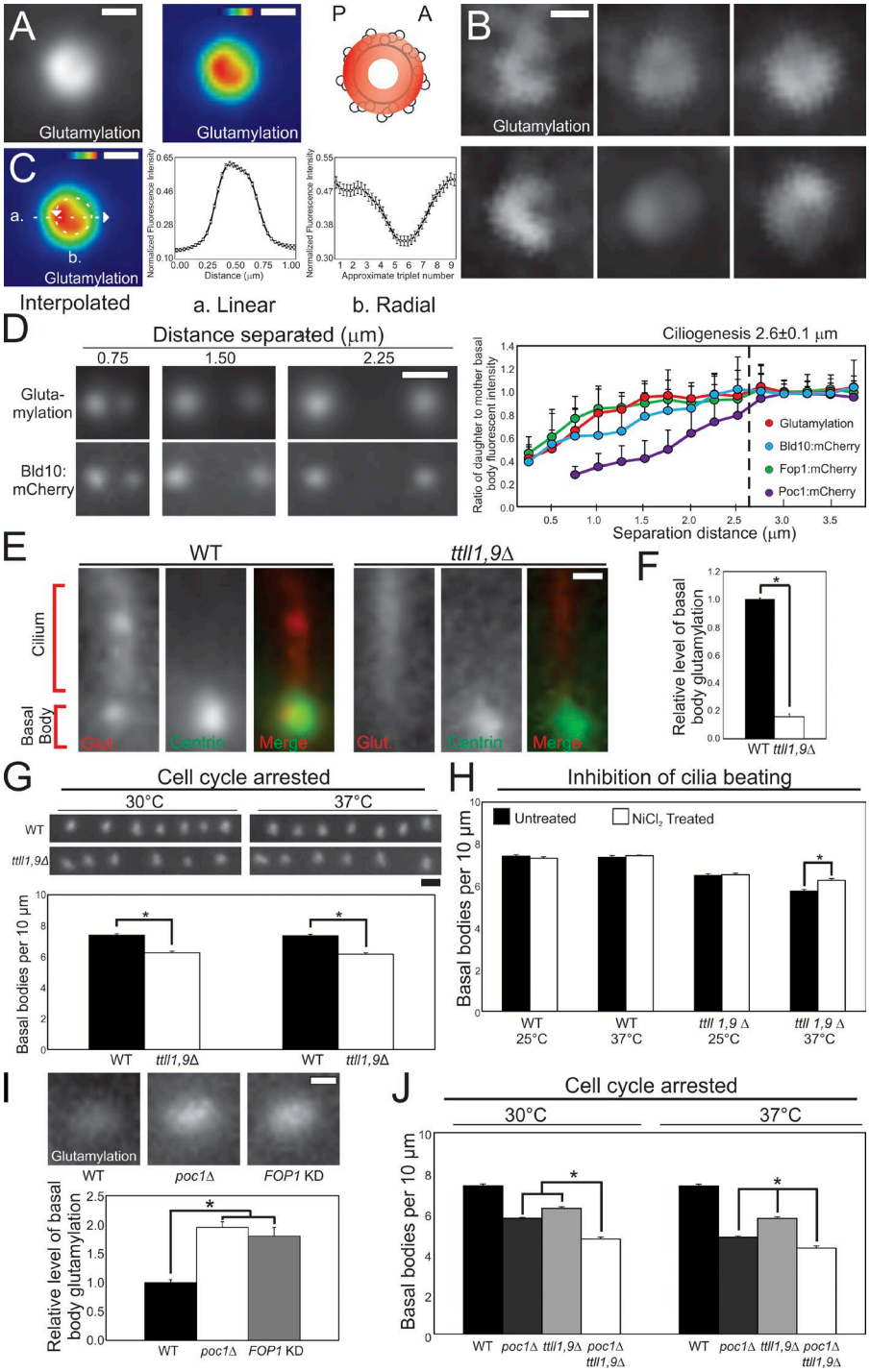

Figure 5. **Microtubule glutamylation stabilizes BBs differentially from BB stability proteins.** (A) SIM imaging reveals that glutamylation is enriched at the posterior and anterior triplet microtubules. (left) Averaged SIM image of BB glutamylation (GT335). *n* = 110 BBs. (middle) Heatmap representation. (right) Schematic localization of BB glutamylation. (B) Representative SIM images showing variable glutamylation in foci and horseshoe patterns at individual BBs. (C, left) Interpolated intensity heatmap of the mean SIM image reveals enrichment of glutamylation at the BB posterior and anterior faces. Quantification of a linear (middle, a.) and radial linescans (left, b.). (A–C) Bars, 0.25 µm. (D) The timing and rate of incorporation of BB glutamylation and Bld10 is similar to Fop1. Glutamylation levels depict the incorporation of glutamylation relative to BB separation. (right) Quantification of BB stability factor and microtubule glutamylation incorporation relative to the mother–daughter BB separation. Bar, 1 µm. (E) BB microtubule glutamylation is significantly reduced in *ttll1,9Δ* cells. BBs and cilia stained for glutamylated microtubules (red) and BBs for centrin (green). Bar, 0.5 µm. (F) Quantification of BB glutamylation levels in WT and *ttll1,9Δ* cells. *n* = 150 BBs. (G, top) Loss of BB microtubule glutamylation causes BB loss. Representative fluorescence images of BB rows in WT and *ttll1,9Δ* cells at 30°C and 37°C in cell cycle–arrested conditions. (bottom) BB frequency in WT and *ttll1,9Δ* cells. *n* = 300 rows. Bar, 1 µm. (H) Inhibition of ciliary beating prevents temperature-induced BB loss in *ttll1,9Δ* cells. Representative BB rows in WT and *ttll1,9Δ* cells in untreated or $NiCl_2$-treated media. *n* = 300 rows. (I) Loss of Poc1 or Fop1 increases BB glutamylation levels. Bar, 0.5 µm. *n* = 150 BBs. (J) Loss of both BB glutamylation and Poc1 increases BB disassembly. Quantification of BB frequency in WT and *ttll1,9Δ*, *poc1Δ* cells at 30°C and 37°C. *n* = 200 BBs. (A–J) Mean ± SEM; *, P < 0.01.

microtubules (Fig. 5, A and B; and Fig. S3, A–D). SIM imaging of individual BBs reveals that glutamylation localizes in horseshoe- and foci-shaped profiles (Fig. 5 B). When averaged, glutamylation is concentrated at the BB posterior face (triplet microtubules 1, 2, 8, and 9) and at the anterior face (triplet microtubule 3, 4, and 5; Fig. 5 C and Fig. S3, A and C), which is consistent with immuno-EM localization (Fig. S3 B). The asymmetric positioning of tubulin glutamylation is not affected by the inhibition of ciliary beating (Fig. S3 C). Additionally, glutamylation is more centrally localized compared with Fop1 (Fig. S3 D). Despite variability in their precise localization, the overall asymmetric distributions of Fop1 and microtubule glutamylation are, to our knowledge, the first characterized molecular asymmetries with respect to the BB microtubule radial axis.

To determine when BB microtubules are glutamylated, we tracked tubulin glutamylation levels during BB maturation relative to the incorporation of BB stability factors (Fig. 5 D). BB glutamylation commences coincident with Fop1 and Bld10 incorporation but earlier than Poc1 incorporation. Furthermore, BB glutamylation incorporates more rapidly than Poc1. These data collectively indicate that the maturation of a stable BB occurs in multiple stages. Thus, asymmetric localizing proteins and PTMs incorporate early during BB maturation, and this is critical for BB stability.

Glutamylation has been reported to both stabilize and destabilize ciliary axonemes, whereas it primarily stabilizes cytoplasmic microtubules and centrioles (Bobinnec et al., 1998a,b, 1999; Wloga et al., 2010). At BBs, it is unknown whether glutamylation stabilizes microtubules against ciliary beating forces. To address this, BB frequency was quantified in cells lacking the two tubulin glutamylases, *TTLL1* and *TTLL9* (*ttll1,9Δ*), which specifically glutamylate BB microtubules but have no measurable effect on axoneme microtubule glutamylation (Fig. 5, E and F; and Fig. S3 E). BB frequency is decreased in cell cycle–arrested and cycling ttll1,9Δ cells (Figs. 5 G and S3 F). Moreover, BB loss in ttll1,9Δ cells is repressed by ciliary inhibition with $NiCl_2$ treatment (Fig. 5 H). The rescue of BB loss by inhibition of ciliary beating suggests that glutamylation, like Poc1 and Fop1, stabilizes BBs against ciliary-dependent forces.

Poc1, Fop1, and microtubule glutamylation act in distinct pathways to stabilize BBs

Poc1 promotes the incorporation of Fop1 during BB maturation, indicating that there is interdependence among the stability factors for their incorporation into BBs. To determine whether such interdependence extends to microtubule glutamylation, BB glutamylation levels were quantified in poc1Δ and *FOP1* knockdown strains. Surprisingly, Poc1 or Fop1 loss increases BB glutamylation, whereas their overexpression decreases glutamylation (Figs. 5 I and S3 G). This suggests that BB glutamylation does not require Poc1 or Fop1. Instead, the increased glutamylation upon Poc1 or Fop1 loss might serve to compensate for BB instability in their absence. Alternatively, loss of Poc1 and Fop1 may promote the accessibility of TTLL modifying enzymes to allow for additional tubulin glutamylation, which facilitates microtubule severing through katanin and spastin (Sharma et al., 2007; Lacroix et al., 2010; Valenstein and Roll-Mecak, 2016). Nonetheless, we find that microtubule glutamylation and BB stability factors have an inverse relationship with respect to their BB incorporation.

If BB glutamylation compensates for the loss of Poc1, then it follows that decreased glutamylation in poc1Δ cells should exacerbate BB instability. To test this hypothesis, and to exclude the possibility that increased glutamylation catalyzes BB instability in stability factor mutants, we created cells that were null for *POC1*, *TTLL1*, and *TTLL9*. Surprisingly, the linear BB frequency in cycling cell *poc1, ttll1, ttll9* triple mutants is increased (Fig. S3 H). However, the total number of BBs per cell is drastically reduced, because the number of ciliary rows is decreased (Fig. S3 I). To specifically test whether existing BBs are less stable in the triple mutant, we assessed BB frequency in cell cycle–arrested cells. At 30°C, the triple mutant cells exhibit a 36%, 18%, and 24% decrease in BB frequency compared with wild-type (WT), poc1Δ, or ttll1,9Δ cells, respectively (Fig. 5 J). Thus, BBs use temporally distinct but functionally overlapping strategies to maintain the normal complement of BBs in the cell.

Conclusion

How BBs manage the mechanical stress imposed upon them by asymmetric ciliary undulations remains poorly understood. This study illuminates an overlapping series of events required for the assembly of stable BBs capable of resisting such stress. These events rely on the timely incorporation of stabilizing proteins and microtubule PTMs at specific domains of the assembling BB. Bld10 and Poc1 symmetrically localize with respect to the BB rotational axis. These BB stability factors exhibit unique incorporation profiles that reflect their distinct functions in assembly and stability. Despite their symmetric localization, loss of triplet microtubules in *bld10Δ* and *poc1Δ* mutants occurs asymmetrically along the plane of ciliary beating, suggesting that these regions experience greater mechanical stress (Bayless et al., 2012; Meehl et al., 2016). Together with the symmetrically localizing stability proteins, Fop1 and microtubule glutamylation reinforce these regions likely by asymmetrically localizing to the radial BB architecture. The coordination between uniquely incorporated and localized stability proteins reveals a dynamic and multidomain architecture of the BB that is responsible for resisting asymmetric ciliary beating.

Materials and methods

T. thermophila cell culture

T. thermophila strains were grown in 2% SPP media (2% protease peptone, 0.2% glucose, 0.1% yeast extract, and 0.003% Fe-EDTA) to mid–log phase at 30°C, unless otherwise indicated. Cells were considered mid–log phase at a density of ∼3×10^5 cells/ml as determined using a Coulter Counter Z1 (Beckman Coulter). All temperature-shift experiments were performed for 24 h. Strains were cell cycle arrested in starvation media (10 mM Tris-HCl, pH 7.4). Perturbations that affect ciliary beating (3% PEO at all temperatures or 250 and 100 µM $NiCl_2$ at 30°C and 37°C, respectively; Larsen and Satir, 1991) were introduced 24 h after cell cycle arrest. The frequency of BBs was quantified 24 h after either PEO or $NiCl_2$ treatment. Ciliary inhibition by $NiCl_2$ treatment was confirmed by reduced cellular swimming.

Mass spectrometry

Proteins isolated by immunoprecipitation were identified by using an ion trap mass spectrometer (LTQ XL; Thermo Fisher Scientific) with a reverse phase gradient over C18 resin (Phenomenex). Analysis was performed using SEQUEST software as described previously (Washburn et al., 2001).

Plasmids

The Fop1:mCherry strain was generated by transforming cells with p4T2-1:FOP1:mCherry. This cassette integrates into the endogenous *FOP1* locus and remains under control of the endogenous promoter. p4T2-1:FOP1:mCherry was generated by PCR amplification of an 825-bp fragment of *FOP1* immediately upstream of the TGA stop codon (5′-CGGGTACCCCATTACTACTCT-3′ and 5′-CGGAATTCT TAATCTTCAACAT-3′) that was cloned into p4T2-1-mCherryLAP to generate p4T2-1-FOP1US-mCherryLAP (Winey et al., 2012). An 807-bp fragment downstream of the TGA stop codon (5′-CGGGAT CCGGATAGCTTTTTT-3′ and 5′-CGGAGCTCTTTGATCTCACAT-3′) was then cloned into p4T2-1-FOP1US-mCherryLAP plasmid intermediate to create p4T2-1FOP1:mCherry. This plasmid contains the *NEO2* drug selection marker. A FOP1:GFP construct was generated as described for p4T2-1FOP:mCherry using the p4T-1-GFPLAP plasmid (Cheeseman and Desai, 2005). The *fop1* knockout cassette was created by replacing the entire *FOP1* open reading frame with the *NEO2* resistance gene. This was achieved by cloning an 835-bp fragment of the *FOP1* 5′ UTR (5′-CGGGTACCCTATTCATCAAAA-3′ and 5′-CGCTCGAGCTGTTCAATATGC-3′) and a fragment of the *FOP1* 3′ UTR (5′-CGGGATCCGGATAGCTTTTTT-3′ and 5′-CGG AGCTCTTTGATCTCACAT-3′) into the p4T2-1 plasmid.

The FOP1 rescue construct (pBSMTTGFP:FOP1) was generated by creating a genomic clone of *GFP* fused to *FOP1* under control

of an inducible MTT promoter (Shang et al., 2002). The 1185-bp *FOP1* cDNA fragment was RT-PCR amplified (5′-CGTACGTAA TGAGAGGATCAC-3′ and 5′-CGACTAGTTCATTAATCTTCAA-3′) and cloned into pBSMTT:GFP:gtw (provided by D. Chalker, Washington University, St. Louis, MO) via a pENTR intermediate. This rescue cassette was transformed into *FOP1* knockdown cells, integrating into the *rpl29* locus.

The overexpression constructs pBSMTTGFP:SAS6a and pBSM TTGFP:POC1 were generated as described for the pBSMTTGFP :FOP1, by PCR amplifying (5′-CGGGATCCGATGGATAGTTTA TC-3′ and 5′-CGAAGCTTTCACTAATTTTTTG-3′, and 5′-CGGGAT CCGATGGCTGCGCCCTGCGCGGA-3′ and 5′-GCAAGCTTTCAT GGTGTTGCTCTCTGCA-3′, respectively). These genomic clones were then cloned into pBSMTTGFPCHX.

Macronuclear transformation

Biolistic transformation was used to transform the p4T2-1-LAP constructs, pBSMTTGFPCHX overexpression constructs, and the *fop1* knockout cassette into the macronucleus of *Tetrahymena* cells (Bruns and Cassidy-Hanley, 2000). 200 µg/ml paromomycin was used to select for the *NEO2* gene, and 7.5 µg/ml cycloheximide was used to select for the *CHX* resistance gene (Gaertig et al., 1994; Hai et al., 2000). To increase the copy number of the endogenously tagged *GFP* and *mCherry* constructs, strains were selectively assorted by incrementally increasing the concentration of paromomycin in the media.

All GFP and mCherry constructs were assorted and maintained with paromomycin concentrations that maintained a strong signal to noise of the fluorescent tag. To ensure equal copy number of LAP constructs in experiments where FOP1:mCherry and POC1 :mCherry levels were assessed in the presence or absence of *POC1* or *FOP1* (Fig. 4 A), respectively, strains were grown at the same paromomycin concentration for multiple passages. In experiments where Sas6a, Poc1, or Fop1 were overexpressed by induction of the MTT promoter and levels of Fop1 or Poc1 were measured, "WT" denotes the identical MTTGFP strains that were not induced with $CdCl_2$ (Fig. 4, B and C).

FOP1 knockdown

Biolistic transformation was used to insert the *fop1* knockout cassette into the macronuclear *FOP1* gene. The entire open reading frame of *FOP1* was targeted and replaced with the *NEO2* gene (Hai et al., 2000). Allelic assortment of the *NEO2* gene was performed by increasing the paromomycin concentration. Increased assortment of the knockout cassette decreases the copy number of WT *FOP1* alleles. Knockdown was verified by genomic PCR (42% reduction) and RT-PCR (58% reduction; Fig. S1, A and B).

Immunoprecipitation

BLD10:mCherryLAP or POC1:mCherryLAP constructs were transformed into B2086 *Tetrahymena* cells. Immunoprecipitation was performed as previously described (Cheeseman et al., 2004; Cheeseman and Desai, 2005). In brief, 2 l of confluent cells (10^6 cells/ml) were washed in PBS and then resuspended in lysis buffer (50 mM Hepes, pH 7.4, 1 mM EGTA, 1 mM $MgCl_2$, 100 mM KCl, 10% glycerol, and 0.05% NP-40) with protease inhibitors. The whole-cell solution was dropped into $LiNi_2$ to produce drops of cell lysate. 5 g of cell drops was ground in a cryogrinder and resuspended in 1.5× lysis buffer and sonicated. Samples were centrifuged at 21,600 *g*, and the supernatant was collected before centrifugation at 135,000 *g*. Samples were immunoprecipitated with α-RFP–coated beads and eluted with 0.1 M glycine, pH 2.6 (Cheeseman et al., 2001).

Light microscopy

Fluorescence imaging was performed as previously described (Bayless et al., 2012) using a Nikon Ti Eclipse inverted microscope with a Nikon 100× Plan-Apochromat numerical aperture 1.4 objective at 25°C. Images were captured with a CMOS camera (Xyla 4.2; Andor Technology). All images were acquired using NIS Elements imaging software (Nikon). Acquisition times ranged between 50 and 500 ms, depending on the experiment. BB frequency was quantified as previously described (Bayless et al., 2012).

Quantification of BB frequency

Quantification of BB frequency was performed by counting the number of BBs along a 10-µm region along a ciliary row in the medial half of the cell. Ciliary rows around the entire circumference of the cell were quantified. All experiments used five measurements per cell over 20 cells. All experiments were repeated in triplicate for a total of 300 counts. All counts were corrected for cell length by multiplying the number of BBs by the ratio of mutant to WT cell length. In cycling cells grown in SPP, only nondividing, stage I cells were selected for analysis. In cell cycle–arrested cells, during cell starvation, a small fraction of cells become arrested in G2; however, the cells that are the focus of this study arrest in G1, assessed by cell size and BB frequency. These G1-arrested cells were used for all BB quantification in starvation experiments.

Immunofluorescence

Immunofluorescence was performed as described previously (Bayless et al., 2012). Cells were washed in PHEM buffer (60 mM 1,4-piperazinediethanesulfonic acid, 25 mM 4-(2-hydroxyethyl)-1-piperazineethanesulfonic acid, 10 mM EGTA, and 2 mM $MgCl_2$, pH 6.9) and then fixed in formaldehyde fixative (3.2% paraformaldehyde and 0.2% Triton X-100, in PHEM buffer) for 5 min. Cells were washed three times in 0.1% BSA in PBS (BSA-PBS) before a 24-h incubation at 4°C with primary antibody diluted in 1.0% BSA-PBS. Primary antibodies used in this study were α-TtCen1 (Stemm-Wolf et al., 2005) and α-glutamylation (GT335; Adipogen; Wolff et al., 1992). Cells were then washed three times in 0.1% BSA-PBS before incubation for 2 h at 25°C in secondary antibody diluted in 1.0% BSA-PBS. Secondary antibodies used in this study were Alexa Fluor 488, 594, or 647 goat α–rabbit IgG, Alexa Fluor 488, 594, or 647 goat α–mouse IgG (Invitrogen). Cells were then washed three times in 0.1% BSA-PBS, and 1 µl of cell pellet was added to coverslip and mounted to a slide with Citifluor mounting media (Ted Pella). Samples were then sealed using clear nail polish.

SIM

SIM imaging was performed using the N-SIM system (Nikon) on a Ti Eclipse inverted microscope equipped with a 100× CF160 Apochromat superresolution/TIRF NA 1.49 objective. Images were captured with an iXon DU897 X3 512 × 512 EMCCD (Andor Technology). Samples were excited using an N-SIM dual band filter cube for 488 and 561 nm excitation. SIM imaging was also performed on a Deltavision OMX Blaze (GE Healthcare) superresolution system. The microscope was equipped with a 60× 1.42 NA point spread function objective. All images were acquired at 25°C using NIS Elements or Deltavision software, respectively. Subtle resolution differences were observed between the N-SIM and OMX Blaze imaging systems. These likely accounted for the improved visualization of glutamylation tubulin fluorescent signal rings with the OMX Blaze system. Image analysis was performed using NIS Elements and ImageJ.

Fluorescence image averaging

Fluorescence averaging was performed using ImageJ's built-in plugins and the ImageJ macro language. To generate the mean fluorescence intensity from widefield images, individual BB rows were rotated along a common anterior–posterior axis and boxes were manually centered over maximum intensity projections of each BB. Once the approximate central position of each BB was identified, boxes were automatically recentered over the highest intensity pixel and used to crop the images. These images were subsequently background subtracted and normalized so that the brightest pixel was set equal to 1. The resulting centered and normalized images were compiled into a new image stack, and the mean intensity image was generated using the mean intensity projection method in ImageJ. The method used to generate the mean fluorescence intensity from SIM images was identical, except the images were all manually centered over the area of lowest intensity within the interior portion of the ring- or horseshoe-shaped signal. To generate the linescans of mean widefield data, a line was centered over the mean BB image, and the resulting pixel intensities were fit to a Gaussian function using the ImageJ curve fitting plugin. To generate linescans of mean SIM data, a line or a circle was centered over the mean ring and the individual pixel intensities across all images were retrieved, which allowed statistical analyses to be performed across the linescan. All linescans were generated without resizing the images. However, some figures show smoothed images that were digitally enlarged with bicubic interpolation and displayed with the ImageJ "physics" lookup table.

Transmission EM

For immuno-EM, a C-terminal FOP1:GFP fusion under endogenous expression was prepared for immuno-EM using high-pressure freezing and freeze substitution (Dahl and Staehelin, 1989; Meehl et al., 2009). Incubation in rabbit-generated α-GFP antibodies, followed by incubation with α-rabbit secondary antibodies conjugated to 15-nm gold particles was used to localize Fop1-GFP. Fop1 was then localized in 60-nm sections by transmission EM. Images were acquired using a CM10 electron microscope (Philips) with a BioScan2 CCD camera (Gatan). For EM analysis of *FOP1* knockdown BB structural defects, *FOP1* knockdown cells were subjected to high-pressure freezing and freeze substitution as previously described (Pearson et al., 2009). Images were acquired using a Tecnai G2 (FEI) equipped with a Gatan Ultrascan digital camera. All images were processed for figures using Corel Draw.

Online supplemental material

Fig. S1 describes genomic and transcript levels of Fop1 in FOP1 knockdown cells, quantification of BB loss in cycling cells, quantification of BB loss with alternative BB markers, histograms of linear BB frequency and ciliary row counts corresponding to Fig. 1 C, and additional examples of FOP1 knockdown transmission EM phenotypes observed in Fig. 1 (D and E). Fig. S2 displays Fop1 localization relative to Cen1, Poc1, and Fop1's N- and C-terminal–tagged proteins, SIM averaging of Fop1 localization using the Deltavision OMX system, the asymmetric shift of Fop1 relative to separation distance between mother and daughter BBs, N-SIM averaged localization of Fop1 after inhibition of ciliary beating ($NiCl_2$ treatment), longitudinal immuno-EM localization of Fop1:GFP, mean timing of ciliogenesis, Cen1:GFP incorporation profile, and quantification of ciliary glutamylation in *ttll1,9Δ* mutants. Fig. S3 displays SIM averaging of glutamylation localization using the Deltavision OMX system, cross section immuno-EM localization of glutamylation, SIM averaged localization of glutamylation after inhibition of ciliary beating, colocalization of averaged Fop1 and glutamylation, quantification of glutamylation levels at the cilium in *ttll1,9Δ* mutants, quantification of BB loss in cycling cell *ttll1,9Δ* mutants, effect of Fop1 and Poc1 overexpression on BB glutamylation levels, and quantification BB frequency and BB row loss in *ttll1,9Δ poc1Δ* triple mutants in cycling cells. Table S1 lists proteomics hits from the Bld10 immunoprecipitation. Table S2 lists proteomics hits from the Poc1 immunoprecipitation. Table S3 lists proteomics hits that were found in both Bld10 and Poc1 immunoprecipitations. Known ribosomal proteins were removed from the lists in Tables S1, S2, and S3.

Acknowledgments

The authors would like to thank Dr. Thomas H. Giddings for EM expertise and Dr. Iain Cheeseman for generous support with discussions and mass spectrometry analyses. We greatly appreciate Dr. Marisa Ruehle for critical comments on the manuscript and Kristin Dahl for generating the *fop1Δ* and FOP1:mCherry constructs. Thanks to Andrew Cahill and Nikon and Robert Moody and GE Healthcare for technical expertise with SIM microscopy.

C.G. Pearson is funded by National Institutes of Health National Institute of General Medical Sciences grant GM099820, the Pew Biomedical Scholars Program, and the Boettcher Foundation. J. Gaertig is funded by National Institutes of Health National Institute of General Medical Sciences grant GM089912.

The authors declare no competing financial interests.

Submitted: 29 April 2016
Revised: 24 August 2016
Accepted: 4 October 2016

References

Abal, M., G. Keryer, and M. Bornens. 2005. Centrioles resist forces applied on centrosomes during G2/M transition. *Biol. Cell.* 97:425–434. http://dx.doi.org/10.1042/BC20040112

Allen, R.D. 1969. The morphogenesis of basal bodies and accessory structures of the cortex of the ciliated protozoan *Tetrahymena pyriformis*. *J. Cell Biol.* 40:716–733. http://dx.doi.org/10.1083/jcb.40.3.716

Bayless, B.A., T.H. Giddings Jr., M. Winey, and C.G. Pearson. 2012. Bld10/Cep135 stabilizes basal bodies to resist cilia-generated forces. *Mol. Biol. Cell.* 23:4820–4832. http://dx.doi.org/10.1091/mbc.E12-08-0577

Bayless, B.A., D.F. Galati, and C.G. Pearson. 2016. *Tetrahymena* basal bodies. *Cilia.* 5:1. http://dx.doi.org/10.1186/s13630-016-0022-8

Bobinnec, Y., A. Khodjakov, L.M. Mir, C.L. Rieder, B. Eddé, and M. Bornens. 1998a. Centriole disassembly in vivo and its effect on centrosome structure and function in vertebrate cells. *J. Cell Biol.* 143:1575–1589. http://dx.doi.org/10.1083/jcb.143.6.1575

Bobinnec, Y., M. Moudjou, J.P. Fouquet, E. Desbruyères, B. Eddé, and M. Bornens. 1998b. Glutamylation of centriole and cytoplasmic tubulin in proliferating non-neuronal cells. *Cell Motil. Cytoskeleton.* 39:223–232. http://dx.doi.org/10.1002/(SICI)1097-0169(1998)39:3<223::AID-CM5>3.0.CO;2-5

Bobinnec, Y., C. Marcaillou, and A. Debec. 1999. Microtubule polyglutamylation in *Drosophila melanogaster* brain and testis. *Eur. J. Cell Biol.* 78:671–674. http://dx.doi.org/10.1016/S0171-9335(99)80053-3

Brinkley, B.R., and J. Cartwright Jr. 1975. Cold-labile and cold-stable microtubules in the mitotic spindle of mammalian cells. *Ann. N. Y. Acad. Sci.* 253(1 The Biology o):428–439. http://dx.doi.org/10.1111/j.1749-6632.1975.tb19218.x

Bruns, P.J., and D. Cassidy-Hanley. 2000. Biolistic transformation of macro- and micronuclei. *Methods Cell Biol.* 62:501–512. http://dx.doi.org/10.1016/S0091-679X(08)61553-8

Cheeseman, I.M., and A. Desai. 2005. A combined approach for the localization and tandem affinity purification of protein complexes from metazoans. *Sci. STKE.* 2005:pl1. http://dx.doi.org/ 10.1126/stke.2662005pl1

Cheeseman, I.M., C. Brew, M. Wolyniak, A. Desai, S. Anderson, N. Muster, J.R. Yates, T.C. Huffaker, D.G. Drubin, and G. Barnes. 2001. Implication of a novel multiprotein Dam1p complex in outer kinetochore function. *J. Cell Biol.* 155:1137–1145. http://dx.doi.org/10.1083/jcb.200109063

Cheeseman, I.M., S. Niessen, S. Anderson, F. Hyndman, J.R. Yates III, K. Oegema, and A. Desai. 2004. A conserved protein network controls assembly of the outer kinetochore and its ability to sustain tension. *Genes Dev.* 18:2255–2268. http://dx.doi.org/10.1101/gad.1234104

Culver, B.P., J.B. Meehl, T.H. Giddings Jr., and M. Winey. 2009. The two SAS-6 homologs in *Tetrahymena thermophila* have distinct functions in basal body assembly. *Mol. Biol. Cell.* 20:1865–1877. http://dx.doi.org/10.1091/mbc.E08-08-0838

Dahl, R., and L.A. Staehelin. 1989. High-pressure freezing for the preservation of biological structure: theory and practice. *J. Electron Microsc. Tech.* 13:165–174. http://dx.doi.org/10.1002/jemt.1060130305

Dippell, R.V. 1968. The development of basal bodies in paramecium. *Proc. Natl. Acad. Sci. USA.* 61:461–468. http://dx.doi.org/10.1073/pnas.61.2.461

Dirksen, E.R. 1971. Centriole morphogenesis in developing ciliated epithelium of the mouse oviduct. *J. Cell Biol.* 51:286–302. http://dx.doi.org/10.1083/jcb.51.1.286

Fouquet, J.P., Y. Prigent, and M.L. Kann. 1996. Comparative immunogold analysis of tubulin isoforms in the mouse sperm flagellum: unique distribution of glutamylated tubulin. *Mol. Reprod. Dev.* 43:358–365. http://dx.doi.org/10.1002/(SICI)1098-2795(199603)43:3<358::AID-MRD10>3.0.CO;2-Y

Gaertig, J., L. Gu, B. Hai, and M.A. Gorovsky. 1994. High frequency vector-mediated transformation and gene replacement in *Tetrahymena*. *Nucleic Acids Res.* 22:5391–5398. http://dx.doi.org/10.1093/nar/22.24.5391

Goto, M., K. Ohki, and Y. Nozawa. 1982. Evidence for a correlation between swimming velocity and membrane fluidity of *Tetrahymena* cells. *Biochim. Biophys. Acta.* 693:335–340. http://dx.doi.org/10.1016/0005-2736(82)90440-0

Hai, B., J. Gaertig, and M.A. Gorovsky. 2000. Knockout heterokaryons enable facile mutagenic analysis of essential genes in *Tetrahymena*. *Methods Cell Biol.* 62:513–531. http://dx.doi.org/10.1016/S0091-679X(08)61554-X

Kunimoto, K., Y. Yamazaki, T. Nishida, K. Shinohara, H. Ishikawa, T. Hasegawa, T. Okanoue, H. Hamada, T. Noda, A. Tamura, et al. 2012. Coordinated ciliary beating requires Odf2-mediated polarization of basal bodies via basal feet. *Cell.* 148:189–200. http://dx.doi.org/10.1016/j.cell.2011.10.052

Lacroix, B., J. van Dijk, N.D. Gold, J. Guizetti, G. Aldrian-Herrada, K. Rogowski, D.W. Gerlich, and C. Janke. 2010. Tubulin polyglutamylation stimulates spastin-mediated microtubule severing. *J. Cell Biol.* 189:945–954. http://dx.doi.org/10.1083/jcb.201001024

Larsen, J., and P. Satir. 1991. Analysis of Ni(2+)-induced arrest of *Paramecium* axonemes. *J. Cell Sci.* 99:33–40.

Le Clech, M. 2008. Role of CAP350 in centriolar tubule stability and centriole assembly. *PLoS One.* 3:e3855. http://dx.doi.org/10.1371/journal.pone.0003855

Lindemann, C.B., A. Orlando, and K.S. Kanous. 1992. The flagellar beat of rat sperm is organized by the interaction of two functionally distinct populations of dynein bridges with a stable central axonemal partition. *J. Cell Sci.* 102:249–260.

Magiera, M.M., and C. Janke. 2014. Post-translational modifications of tubulin. *Curr. Biol.* 24:R351–R354. http://dx.doi.org/10.1016/j.cub.2014.03.032

Marshall, W.F., and C. Kintner. 2008. Cilia orientation and the fluid mechanics of development. *Curr. Opin. Cell Biol.* 20:48–52. http://dx.doi.org/10.1016/j.ceb.2007.11.009

Meehl, J.B., T.H. Giddings Jr., and M. Winey. 2009. High pressure freezing, electron microscopy, and immuno-electron microscopy of *Tetrahymena thermophila* basal bodies. *Methods Mol. Biol.* 586:227–241. http://dx.doi.org/10.1007/978-1-60761-376-3_12

Meehl, J.B., B.A. Bayless, T.H. Giddings Jr., C.G. Pearson, and M. Winey. 2016. *Tetrahymena* Poc1 ensures proper intertriplet microtubule linkages to maintain basal body integrity. *Mol. Biol. Cell.* 27:2394–2403. http://dx.doi.org/10.1091/mbc.E16-03-0165

Mikolajka, A., X. Yan, G.M. Popowicz, P. Smialowski, E.A. Nigg, and T.A. Holak. 2006. Structure of the N-terminal domain of the FOP (FGFR1OP) protein and implications for its dimerization and centrosomal localization. *J. Mol. Biol.* 359:863–875. http://dx.doi.org/10.1016/j.jmb.2006.03.070

Nanney, D.L. 1971. The pattern of replication of cortical units in *Tetrahymena*. *Dev. Biol.* 26:296–305. http://dx.doi.org/10.1016/0012-1606(71)90128-X

Nanney, D.L., and M. Chow. 1974. Basal body homeostasis in *Tetrahymena*. *Am. Nat.* 108:125–139. http://dx.doi.org/10.1086/282890

O'Toole, E.T., and S.K. Dutcher. 2014. Site-specific basal body duplication in *Chlamydomonas*. *Cytoskeleton (Hoboken).* 71:108–118. http://dx.doi.org/10.1002/cm.21155

Pearson, C.G. 2014. Choosing sides--asymmetric centriole and basal body assembly. *J. Cell Sci.* 127:2803–2810. http://dx.doi.org/10.1242/jcs.151761

Pearson, C.G., D.P. Osborn, T.H. Giddings Jr., P.L. Beales, and M. Winey. 2009. Basal body stability and ciliogenesis requires the conserved component Poc1. *J. Cell Biol.* 187:905–920. http://dx.doi.org/10.1083/jcb.200908019

Riedel-Kruse, I.H., A. Hilfinger, J. Howard, and F. Jülicher. 2007. How molecular motors shape the flagellar beat. *HFSP J.* 1:192–208. http://dx.doi.org/10.2976/1.2773861

Satir, P., T. Heuser, and W.S. Sale. 2014. A structural basis for how motile cilia beat. *Bioscience.* 64:1073–1083. http://dx.doi.org/10.1093/biosci/biu180

Shang, Y., X. Song, J. Bowen, R. Corstanje, Y. Gao, J. Gaertig, and M.A. Gorovsky. 2002. A robust inducible-repressible promoter greatly facilitates gene knockouts, conditional expression, and overexpression of homologous and heterologous genes in *Tetrahymena thermophila*. *Proc. Natl. Acad. Sci. USA.* 99:3734–3739. http://dx.doi.org/10.1073/pnas.052016199

Sharma, N., J. Bryant, D. Wloga, R. Donaldson, R.C. Davis, M. Jerka-Dziadosz, and J. Gaertig. 2007. Katanin regulates dynamics of microtubules and biogenesis of motile cilia. *J. Cell Biol.* 178:1065–1079. http://dx.doi.org/10.1083/jcb.200704021

Stemm-Wolf, A.J., G. Morgan, T.H. Giddings Jr., E.A. White, R. Marchione, H.B. McDonald, and M. Winey. 2005. Basal body duplication and maintenance require one member of the *Tetrahymena thermophila* centrin gene family. *Mol. Biol. Cell.* 16:3606–3619. http://dx.doi.org/10.1091/mbc.E04-10-0919

Valenstein, M.L., and A. Roll-Mecak. 2016. Graded control of microtubule severing by tubulin glutamylation. *Cell.* 164:911–921. http://dx.doi.org/10.1016/j.cell.2016.01.019

Vernon, G.G., and D.M. Woolley. 2004. Basal sliding and the mechanics of oscillation in a mammalian sperm flagellum. *Biophys. J.* 87:3934–3944. http://dx.doi.org/10.1529/biophysj.104.042648

Washburn, M.P., D. Wolters, and J.R. Yates III. 2001. Large-scale analysis of the yeast proteome by multidimensional protein identification technology. *Nat. Biotechnol.* 19:242–247. http://dx.doi.org/10.1038/85686

Winey, M., A.J. Stemm-Wolf, T.H. Giddings Jr., and C.G. Pearson. 2012. Cytological analysis of *Tetrahymena thermophila*. *Methods Cell Biol.* 109:357–378. http://dx.doi.org/10.1016/B978-0-12-385967-9.00013-X

Wloga, D., K. Rogowski, N. Sharma, J. Van Dijk, C. Janke, B. Eddé, M.H. Bré, N. Levilliers, V. Redeker, J. Duan, et al. 2008. Glutamylation on α-tubulin is not essential but affects the assembly and functions of a subset of microtubules in *Tetrahymena thermophila*. *Eukaryot. Cell.* 7:1362–1372. http://dx.doi.org/10.1128/EC.00084-08

Wloga, D., D. Dave, J. Meagley, K. Rogowski, M. Jerka-Dziadosz, and J. Gaertig. 2010. Hyperglutamylation of tubulin can either stabilize or destabilize microtubules in the same cell. *Eukaryot. Cell.* 9:184–193. http://dx.doi.org/10.1128/EC.00176-09

Wolff, A., B. de Néchaud, D. Chillet, H. Mazarguil, E. Desbruyères, S. Audebert, B. Eddé, F. Gros, and P. Denoulet. 1992. Distribution of glutamylated α and β-tubulin in mouse tissues using a specific monoclonal antibody, GT335. *Eur. J. Cell Biol.* 59:425–432.

Yan, X., R. Habedanck, and E.A. Nigg. 2006. A complex of two centrosomal proteins, CAP350 and FOP, cooperates with EB1 in microtubule anchoring. *Mol. Biol. Cell.* 17:634–644. http://dx.doi.org/10.1091/mbc.E05-08-0810